Nonlinear Tolerant Spectrally-Efficient Transmission Using PDM 64-QAM Single Carrier FDM With Digital Pilot-Tone

Takayuki Kobayashi, *Member, IEEE*, Akihide Sano, *Member, IEEE*, Akihiko Matsuura, Yutaka Miyamoto, *Member, IEEE*, and Koichi Ishihara, *Member, IEEE*

(Invited Paper)

***Abstract*—We propose nonlinear tolerant single carrier frequency-division-multiplexing (SC-FDM) signal enhanced by digital pilot-tone for future high speed Ethernet transport like 400 G Ethernet. First, we discuss system configuration and the wavelength-division-multiplexed (WDM) transmission of SC-FDM signals employing polarization-division-multiplexed (PDM) 64-ary quadrature amplitude modulation (64-QAM). Next, we describe the long-haul transmission characteristics of 50 GHz-spaced 538 Gb/s $\times$ 7 ch WDM signals. We compare digital back-propagation (DBP) and digital pilot-tone for nonlinearity compensation and experimentally show that digital pilot-tone can effectively compensate the phase noise induced by inter-channel nonlinear effects with less computational complexity than DBP. Then we discuss a high-capacity transmission experiment employing 548 Gb/s PDM-64QAM SC-FDM; 102.3 Tb/s (224 $\times$ 548 Gb/s) C- and extended L-band WDM transmission is demonstrated over 240 km (3 $\times$ 80 km) of pure-silica-core fiber (PSCF) with all-Raman amplification. Thanks to the high nonlinear tolerance enhanced by pilot-tone, we can employ the 80 km repeater spacing used in conventional terrestrial systems. Assuming 20% forward error correction (FEC) overhead, a spectral efficiency of 9.1 b/s/Hz is achieved.**

***Index Terms*—Digital signal processing, fiber-optic transmission systems, 400 G Ethernet transport, quadrature amplitude modulation (QAM), single- carrier frequency-division multiplexing (SC-FDM).**

I. Introduction

RESEARCH interest is moving from 100 G transport systems to higher-speed channel transport for accommodating future client signals such as 400 GE on optical transport networks (OTNs). When conventional optical transport systems are upgraded, it is important to enhance the capacity while maintaining compatibility with today's terrestrial network system specifications such as 50/100 GHz WDM spacing and $\sim$100 km repeater spacing [1]. High-order Quadrature amplitude modulation (QAM) is indispensable to ensure compatibility with the conventional 100 G transport system with 50 GHz-WDM spacing [2]–[4]. However the baud rate and the order of QAM are constrained mainly by the operating speed of electrical devices such as digital-to-analogue converters (DACs) and analogue-to-digital converters (ADCs). Therefore, the 400-Gb/s class channel is achieved by multiplexing several high-order QAM signals in the optical frequency domain; such multiplexed signal is often called super channel [5]. Both single-carrier and multi-carrier techniques are investigated for the modulation of each optical subcarrier. OFDM is a promising candidate and has flexibility and high spectral efficiency with many subcarriers. It also makes it easy to embed pilot signals to estimate the transfer function of the transmission line and compensate impairments [6], [7]. 400 Gb/s/ch transmission experiments have been reported that use multi-band OFDM with high-order QAM [3], [8]. An OFDM signal with many subcarriers has high peak-to-average power ratio (PAPR) [9], and its nonlinear tolerance was less than that of the single-carrier equivalent [10]–[12]. Single carrier frequency division multiplexing (SC-FDM) is an attractive candidate and was originally proposed to avoid nonlinear signal distortion in electrical power amplifiers in wireless communication systems [13]. It was introduced to uplink transmission in 3 GPP long term evolution (LTE) for PAPR reduction. Similarly, SC-FDM is also promising for suppressing the nonlinear phenomena of optical transmission fiber. Studies on the fiber nonlinearities when SC-FDM is applied to fiber transmission [11], [14], [15] have been reported. DFT-spread-OFDM, where signal generation and detection with digital signal processing is based on the system in wireless communication, was utilized in their investigations. And 32/64-QAM hybrid SC-FDM signal transmission assisted by training sequences has been reported by AT&T [4]. In this paper, we define the SC-FDM signal as the super channel consisting of Nyquist-pulse-shaped single carrier signals without DFT-spread OFDM processing.

Another important issue is to consider the trade-off between the number of signal points of M-QAM and required OSNR. In high-order QAM transmission, low-noise optical amplifiers such as all-Raman amplifiers and advanced forward error correction (FEC) [16], [17], which requires extra overhead (more

Manuscript received May 11, 2012; revised July 03, 2012; accepted July 07, 2012. Date of publication July 23, 2012; date of current version December 12, 2012. This work was supported in part by the National Institute of Information and Communications Technology (NICT), Japan.

The authors are with NTT Network Innovation Laboratories, NTT Corporation, Yokosuka, Kanagawa, 239-0847 Japan (e-mail: kobayashi.takayuki@lab.ntt.co.jp).

Color versions of one or more of the figures in this paper are available online at http://ieeexplore.ieee.org.

Digital Object Identifier 10.1109/JLT.2012.2208619

than 20%), are indispensable. Assuming over 20% FEC overhead, the required line rate for 400 Gb/s client signal will be more than 500 Gb/s. With 50 GHz-WDM spacing, a spectral efficiency (SE) of 10 bps/Hz is needed.

Nonlinearity compensation is a promising technique to increase the fiber launched power and achieve high OSNR. So far, several nonlinearity compensation techniques have been proposed and investigated [18]–[24]. Digital back-propagation (DBP) is a straightforward nonlinearity compensation technique, and it has been intensively investigated for various modulation formats [18]–[21]. It is implemented by repeating small steps of chromatic dispersion compensation and phase rotation in proportion to the square of the received electrical fields. Ideally, DBP can compensate intra- and inter-channel nonlinear effects including self phase modulation (SPM), cross-polarization modulation (XpolM), cross phase modulation (XPM) and four wave mixing (FWM). In practice, if inter-channel effects are compensated by DBP, the coherent receiver must capture the total electrical fields, including not only the target channel but also neighboring channels. Therefore, available capture bandwidth in DBP is limited by the operation speeds of electrical devices such as ADCs and digital signal processing units (DSPs). This complicates the compensation of inter-channel nonlinearity by DBP [25]. The DBP technique has powerful performance against intra-channel nonlinearity and can be applied to any modulation format; however, one disadvantage is its high computational complexity; the calculation cost increases with transmission distance and step size resolution [22].

An attractive method for inter-channel nonlinear effects is to utilize the phase information from a pilot-tone attached to the main signal. Pilot-tone is affected by nearly the same impairments as the main signal from neighboring channels; phase noise due to nonlinear effects and laser line width can be estimated without neighboring channel information. In optical OFDM systems, some subcarriers can be easily utilized to carry the pilot signal. Phase noise compensation by pilot-tone for optical OFDM system, which is generated by DC-bias control, was proposed in [7]. For optical OFDM systems, experiments on the compensation of phase noise induced by laser linewidth [7] and by XPM [26], [27] have been reported. Recently, we experimentally applied pilot-tone to a single carrier system to enhance its nonlinear tolerance for the first time and demonstrated 45.2 Tb/s C-band WDM transmission over 240 km [2]. Another group reported the numerical investigation of PDM-16QAM with pilot-tone [28].

Fig. 1 compares the circuit size of DBP and pilot-tone. Circuit size is taken as the number of NAND gates, which are required by each compensation technique, as a function of transmission distance. The numbers of NAND gate are estimated from the total number of multiplication operations and Flip-Flops in the same way as used in [22]. For circuit size estimation, we employ the function blocks shown in the inset of Fig. 1. Iteration count of $\mathrm{N_{span}}$ for DBP was set to the number of 80 km spans used. To ensure a fair comparison, the estimated circuit size of pilot-tone also includes a fixed frequency domain equalizer (FDE) for CD compensation [29]. We can see that the circuit size of pilot-tone aided technique has almost constant while that of DBP increases

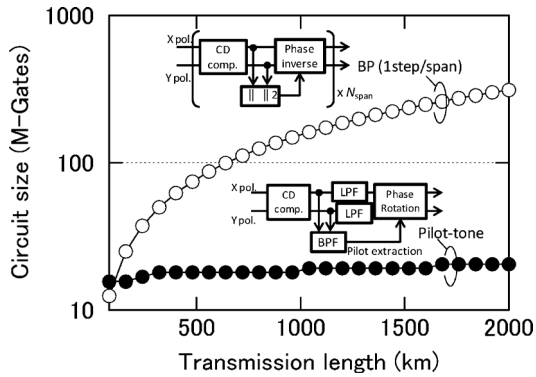

Fig. 1. Circuit size comparison of DBP method and pilot-tone method.

drastically. This circuit size is estimated assuming simple implementation. Recently, the modified DBP to reduce computational complexity has been investigated [20]. For transmission distances greater than 80 km, the pilot-tone aided technique has much smaller circuit size than that of DBP. For experimental example, using pilot-tone, we achieved Q-improvement by 0.5 dB in 90 ch WDM configuration [2]. It shows inter-channel XPM can be partly compensated with pilot-tone aided technique. On the other hand, improving Q of 1 dB was achieved after 1200 km through SPM compensation based on the DBP in single channel configuration [30]. Although nonlinear effect compensated by each technique is different, pilot-tone-aided technique is attractive to enhance the transmission performance when considering the computational costs against amount of Q-improvement.

In this paper, we propose and discuss PDM 64-QAM SC-FDM with pilot-tone for 400-Gb/s-class high speed channel transport. In Section II, we describe the configuration and digital signal processing function of the transmitter and receiver for SC-FDM signals enhanced by digital pilot-tone aided phase noise compensation. Section III discusses the long-haul transmission characteristics of 538-Gb/s SC-FDM signals in the 50-GHz-spaced 7 ch WDM configuration which utilizes 80.1-km-span pure silica core fiber with all-Raman amplification [31]. The nonlinearity compensation performance of pilot-tone and DBP is experimentally investigated. In Section IV, the feasibility of a 100 Tb/s-class transport system, which can accommodate high speed client signals of 400 G Ethernet with standard terrestrial repeater spacing of 80 km and WDM spacing of 50 GHz, is examined in high capacity transmission experiments; 102.3 Tb/s transmission is demonstrated over 3×80 km of PSCF by employing 548-Gb/s PDM-64QAM SC-FDM signals with pilot-tone and 11.2-THz ultra-wideband low-noise amplification in the C- and extended L-bands [32]. Finally, we conclude in Section V.

II. Single Carrier FDM With Digital Pilot-Tone

A. Generation of SC-FDM Signal With Pilot-Tone

Fig. 2 shows the transmitter configuration that generates a SC-FDM signal. Its key feature is enhancing the phase noise tolerance of the single carrier signal by attaching pilot-tone to each subcarrier. The transmitter consists of multi-carrier source, optical (de-)multiplexer, parallel IQ-modulators and

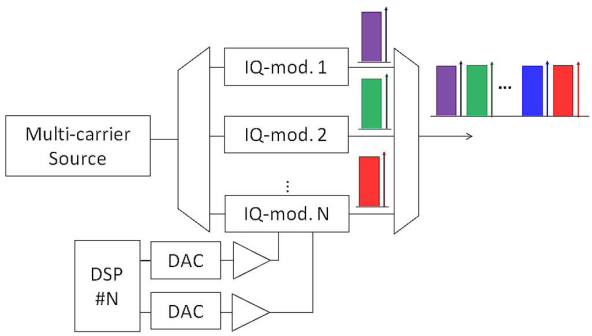

Fig. 2. Concept of SC-FDM transmitter with digital pilot-tone.

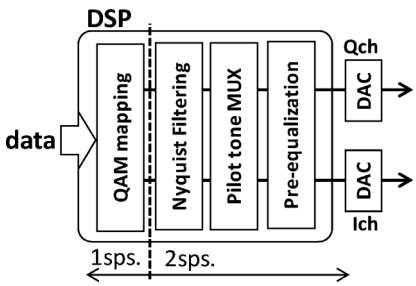

Fig. 3. DSP Block diagram at transmitter.

their driving DACs with DSP units. Such parallelized structure is often employed to mitigate the operation speed limits of electrical devices and generate higher bit-rate channels [10]. The SC-FDM transmitter requires DACs and DSP units to achieve spectrally-efficient high-order QAM signals whose spectrum is rectangular (Nyquist-pulse shaping with a small roll-off factor), and to add the pilot-tone in a fully digital domain. Frequency-locked optical carriers from the multi-carrier source are separated and each carrier is individually modulated by an IQ-modulator driven by a Nyquist-pulse-shaped electrical QAM signal with pilot tone. Next, they are coupled to achieve the SC-FDM signal. The benefit of our SC-FDM scheme is that pilot-tone insertion has little impact on the main signal because the signal component around the pilot-tone is tightly suppressed by Nyquist pulse shaping. Because frequency-locked optical carriers and sharp Nyquist-pulse-shaping help to avoid linear cross-talk between neighboring subcarriers, subcarrier spacing can be close without concern for the frequency fluctuation of lasers.

DSP block diagram for generating the electrical QAM signal used to drive the IQ-modulator is shown in Fig. 3. First, input data is mapped to QAM constellation and then up-sampled to 2 samples/symbol (2 sps). Up-sampled data is pulse-shaped with Nyquist-filter with the small roll-off factor of $\sim$0.1. A sinusoidal pilot tone is simply added to the frequency band attenuated by the tight Nyquist-filter. Finally, the electrical QAM signal is pre-equalized to mitigate the band-limiting effect of the transmitter and receiver, and fed to the DACs.

B. Demodulation Scheme for SC-FDM Employing M-QAM

The receiver configuration and DSP block functions including pilot-tone aided phase noise compensation are shown in Fig. 4. Each subcarrier in the SC-FDM signal is individually

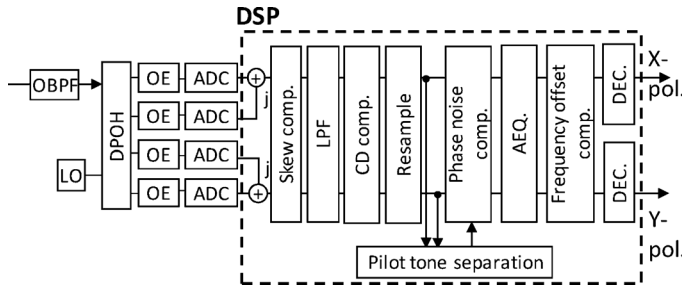

Fig. 4. Coherent receiver configuration and demodulation algorithm.

demodulated. Subcarrier separation can be realized with an optical bandpass filter and digital low pass filter. The received signals are filtered by optical bandpass filter (OBPF), and detected by a polarization-diversity intradyne receiver containing a PLC-based dual polarization optical hybrid (DPOH). Real and imaginary parts of the two polarization tributaries are detected by four balanced photo detectors, and digitized by ADCs. In our experiments, high speed digital storage oscilloscopes were used instead of ADCs. The received data were stored in sets of a few M samples and post-processed off-line. After skew compensation and anti-aliasing with a digital low pass filter, chromatic dispersion (CD) was compensated by overlap FDE [29]. The signal is then re-sampled to 2 sps. Phase noise compensation is performed by the digital pilot-tone which is extracted from the main signals as described in the next section. Polarization de-multiplexing and signal equalization were realized by a T/2-spaced adaptive equalizer (AEQ) with butterfly configuration. Carrier frequency offset was compensated by a frequency offset compensator based on the digital PLL technique [33]. Our adaptive signal processing procedure is divided into 4 steps. The first step consists of pre-convergence by CMA-multi-modulus algorithm (MMA) [34] to polarization de-multiplexing and channel equalization. In this step, because the PLL is off, the constellation is rotated due to frequency offset. In the second step and third steps, the AEQ control algorithm is unchanged from CMA-MMA. PLL starts to perform coarse frequency offset compensation. Phase detection is based on the sign of decided symbols. When constellation rotation is almost stopped, the phase detector is switched to decision-directed mode. In the fourth step, the adaptive filter control algorithm is switched to DD-LMS [35] in order to improve the SNR. This approach yields good and stable convergence. This is easily applied to M-QAM by altering the decision circuits and parameters.

C. Pilot-Tone Aided Phase Noise Compensation

A pilot-tone aided phase noise compensation technique for optical OFDM was proposed by Jansen *et al.* [7]. We applied this technique to a single carrier optical signal. This paper utilizes the pilot-tone for compensation of phase noise generated by nonlinear effects between neighboring signals. The pilot-tone is impaired by nearly the same nonlinear effects as the main signal, so the phase noise due to XPM from neighboring signals, such as WDM channels and subcarriers in SC-FDM signal, can be estimated from the pilot-tone. Simple implementations of pilot-tone extraction and phase noise compensation shown in Fig. 5

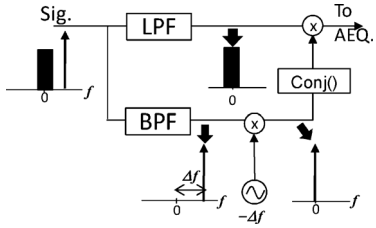

Fig. 5. Implementation of pilot-tone aided phase noise compensator.

are utilized in all experiments. The pilot tone was separated from the single carrier signal with a digital BPF and frequency-shifted to zero frequency. The extracted pilot tone was complex-conjugated, and then multiplied against the main signal [7]. In our demodulation algorithm, the compensated signal is fed into the AEQ block. The capability of pilot-tone aided phase noise compensation depends on the pilot-to-signal ratio (PSR) and bandwidth of BPF for pilot-tone extraction. The PSR is defined as $10\log_{10}(\mathrm{P_{pilot}}/\mathrm{P_{sig}})$ where $\mathrm{P_{pilot}}$ and $\mathrm{P_{sig}}$ represent the power of the pilot tone and the single carrier signal; their powers were measured before the pre-equalization block in transmitter DSP units. Low PSR and wide BPF bandwidth enhance phase noise, while high PSR decreases main signal SNR. A trade-off exists between noise enhancement and phase noise compensation [27]. Optimal bandwidth of BPF and PSR are described in the following section.

III. Long-Haul WDM Transmission of a 538 Gb/s PDM 64-QAM SC-FDM Signals

This section details the long-haul transmission characteristics of 538-Gb/s SC-FDM signals in 50-GHz-spaced 7 ch WDM configuration. Transmission line is a re-circulating loop containing three 80 km-span PSCF without inline dispersion compensation. The nonlinearity compensation techniques of pilot-tone and DBP are experimentally investigated using the same configuration.

A. Experimental Setup

Fig. 6 shows the transmitter for 538 Gb/s PDM 64-QAM SC-FDM signal. An optical carrier from laser diode (LD) was passed through a Mach- Zehnder modulator (MZM) driven by a dual-frequency electrical signal to achieve 12.5-GHz spaced 4 subcarriers [36]. The driving signal consisted of the frequencies of 6.25 GHz and 18.75 GHz. A Mach–Zehnder interferometer (MZI) with 12.5-GHz FSR and interleaving filter were also employed to suppress the spurious components below 40 dB (Fig. 7(a)). Each subcarrier was simultaneously modulated by an IQ-modulator (IQ-mod1) driven by an electrical Nyquist-pulse-shaped 5.6-Gbaud 64QAM signal with pilot-tone. We performed off line processing shown in Fig. 3, to generate the electrical signal driving IQ-mod1. An 8-level data sequence with length of $2^{15}-1$ was created by combining three delayed copies of a $2^{15}-1$ pseudo-random binary sequence (PRBS). Raised cosine filter with a roll-off factor of 0.1 was employed. To avoid an additional penalty by filtering, tap number of the pulse-shaping filter was set to 1024. Pre-processed data was uploaded to an arbitrary waveform generator (AWG) that was operated at 11.2 Gsamples/s with 10 bit resolution. This corresponds to 2 times oversampling. The 12.5-GHz-spaced 4-subcarrier signal and its 6.25 GHz-frequency-shifted signal by IQ-mod2 were combined by the optical coupler shown in Fig. 7(b), to achieve a 538-Gb/s SC-FDM signal after polarization multiplexing. It consisted of eight 6.25 GHz-spaced 64-QAM signals. Delay T was set to about 9.5 nsec. A pilot-tone was attached to each subcarrier (located at 3 GHz from the center frequency of the subcarrier). Its electrical spectra, which were calculated from the received signal by coherent detection, are shown in Fig. 7(c).

Fig. 8 shows the experimental setup for long-haul transmission with re-circulating loop. Seven lasers were operated on a 50 GHz grid from 1548.5 nm to 1550.92 nm. We used a tunable external-cavity laser (ECL) with a linewidth of about 60 kHz for the test channel; the remaining lasers were DFB lasers (linewidth $\sim$2 MHz). The odd/even optical carriers were separately multiplexed, and each carrier was passed through the SC-FDM transmitter described in Fig. 6. AWGs in $\mathrm{T}\times 1$ and $\mathrm{T}\times 2$ were independently driven by different pre-processed data. Optical bandpass filter (OBPF) was inserted to suppress ASE noise at out-of-band of 7 ch WDM signals. Polarization multiplexing was done by splitting the signal into two copies, delaying one signal by 25 nsec. The transmission line consisted of a 240.3 km re-circulating loop containing three 80.1-km spans of low-loss and low-nonlinear PSCF. Its loss coefficient was 0.169 dB/km and its $\mathrm{A_{eff}}$ was 110 $\mu\mathrm{m}^2$. Furthermore, chromatic dispersion was 21.1 at 1563 nm; PMD was 0.078 ps/km$^{1/2}$. Inline dispersion compensation was not used. We utilized all-Raman amplification to improve the OSNR; the backward pumped distributed Raman amplifiers (DRA) yielded the on-off gain of 16 dB. An erbium-doped fiber amplifiers (EDFA) was utilized to compensate the loss of optical components such as AOM switches, optical coupler, and loop synchronous polarization scrambler (LSPS). Its noise figure was $\sim$5 dB. Coherent receiver setup is the same as shown in Fig. 4. In this experiment, we employed 0.5-nm and 0.1-nm OBPFs, and used a free-running ECL with a linewidth of $\sim$70 kHz as the LO. The received data was digitized at 80 GS/s using two synchronized digital storage oscilloscopes, and stored in sets of 4 M samples. Received signals were post-processed offline using the algorithm described in Section II. Bit error ratio (BER) was calculated from the 1.5 Mbit demodulated signals.

B. Back-to-Back Measurements

The measured OSNR tolerance of a single carrier 67.2-Gb/s signal and 8-subcarrier 538-Gb/s SC-FDM signal are shown in Fig. 9. Their required OSNRs for the BER of 1×10^{-3} are 22 dB and 31 dB. The excess OSNR penalty due to subcarrier multiplexing was less than 0.1 dB at the range of BER from 10^{-3} to 10^{-2}, thanks to the suppression of spurious components and Nyquist filtering with roll-off factor of 0.1. These BER curves were calculated using the pilot-tone. At high OSNRs ($>$40 dB), it slightly decreased the error floor, because phase noise induced by laser line width was partly compensated. At around low OSNR values, which were achieved after transmission, improvement of OSNR tolerance was not observed. Fig. 10 shows the subcarrier dependence of Q-factor in a single channel and

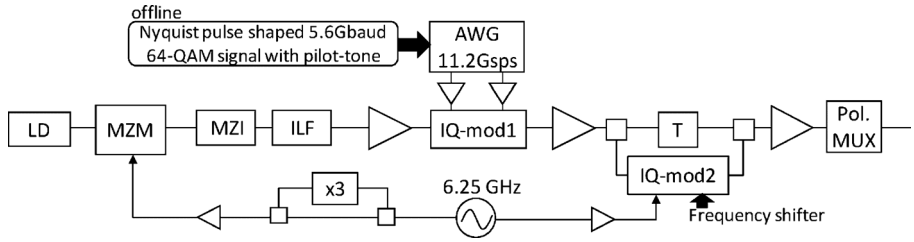

Fig. 6. Transmitter configuration for a single 538-Gb/s PDM 64QAM SC-FDM signal.

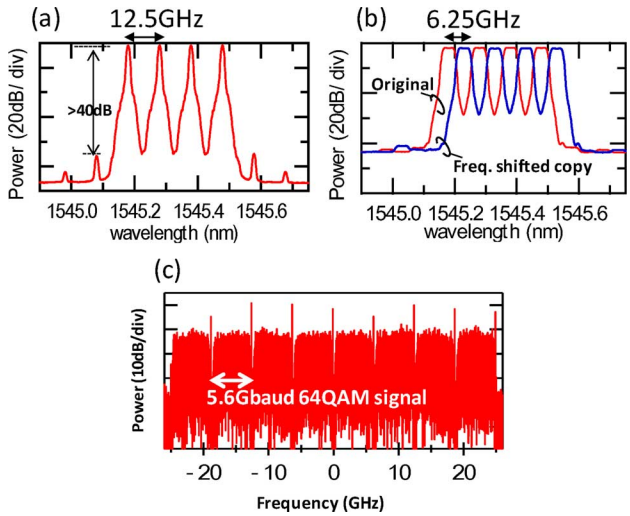

Fig. 7. Signal spectrum at transmitter. (a) Optical spectrum at ILF output. (b) Optical spectrum at IQ-mod1. (c) Electrical spectrum of a single 538 Gb/s 8-subcarrier SC-FDM signal.

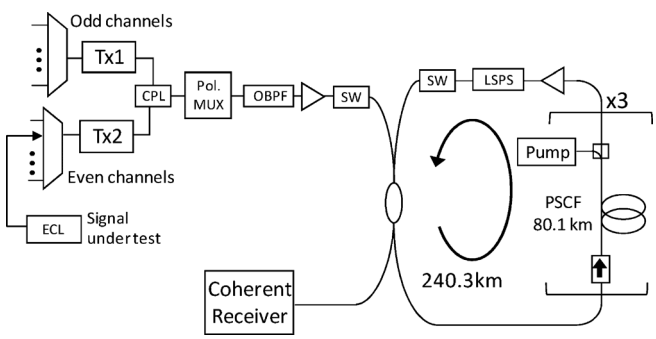

Fig. 8. Experimental setup for 7 × 538 Gb/s 50-GHz-spaced WDM long-haul transmission.

WDM configuration at the OSNR of 31 dB. In single channel measurement, the subcarrier at the edges of SC-FDM signal showed higher Q-factor due to the absence of any neighboring subcarrier.

C. Characteristics of Pilot-Tone-Aided Phase Noise Compensation for WDM Transmission

In this measurement, we investigated the optimal parameters of pilot-tone aided phase noise compensation in 7 ch WDM long-haul transmission. A comparison of DBP and pilot-tone-aided method for nonlinearity compensation was also conducted.

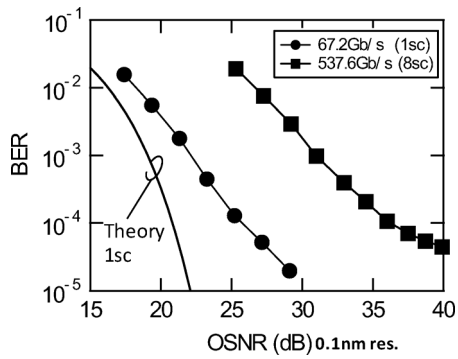

Fig. 9. OSNR tolerance of 538 Gb/s SC-FDM signal at back-to-back configuration.

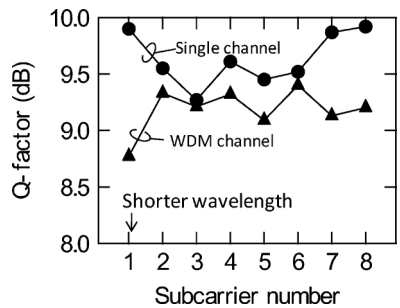

Fig. 10. Dependence of Q-factor on subcarriers in single channel 538 Gb/s SC-FDM signal.

First, optimal PSR was investigated for the three transmission distances of 240 km, 480 km and 720 km. The test wavelength was 1550.12 nm, ch5. PSR was varied from -28 dB to -4 dB and the fiber launched power was fixed to -3.5 dBm/ch. Total power of pilot-tone and signal was set constant. As increasing the PSR for accurate phase compensation, the power of main signal is decreased and OSNR is degraded because the total power is constant. To investigate the balance of them, we used the same launched power for different PSR. Fig. 11 shows Q-factors as a function of PSR at each distance. At lower PSR, Q-factors were decreased by the pilot-tone aided phase noise compensation because phase estimation via pilot-tone is less accurate due to influence of ASE noise. At higher PSRs, on the other hand, Q-factor degradation was caused by OSNR decrease. As transmission distance increases, the peak of the Q-factors strengthens because accumulated inter-channel nonlinear effects such as XPM are effectively compensated by the pilot-tone. We found the optimal PSR to be around -14 dB. In the following experiments, PSR is set to -14 dB.

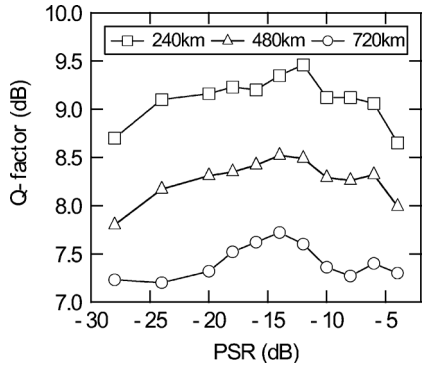

Fig. 11. Q-factor as a function of PSR in 7 ch WDM configuration.

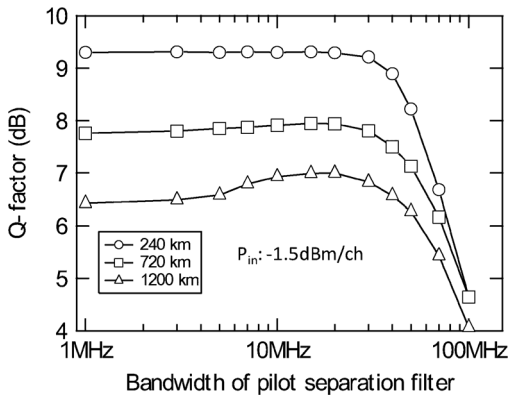

Fig. 12. Band-pass filter optimization for pilot-tone extraction.

The bandwidth of BPF for pilot-tone extraction is also an important parameter. Fig. 12 shows the result of BPF optimization for long-haul transmission. This measurement was conducted using 7 ch WDM configuration. The test wavelength was 1550.12 nm, ch5. PSR was set to -14 dB. The fiber launched power was fixed to -1.5 dBm to conduct the measurements under high nonlinearity. In this experiment, we employed a third-order Gaussian filter as BPF and half width at half maximum (HWHM) was varied from 1 MHz to 100 MHz. At the transmission distance of 1200 km, which strengthens the accumulation of inter-channel nonlinear effects, the Q-factor curve has a peak at the bandwidth of 15 MHz. At BPF bandwidth over 30 MHz, Q-factors were rapidly degraded because of the noise enhancement yielded by the wide bandwidth of the BPF.

We compared our proposal to DBP using 7 ch 50-GHz-spaced WDM configuration. When DBP was applied to receive data, we utilized the multi-stage nonlinear equalizer [21] which is shown in the inset of Fig. 1, instead of the CD compensator. The DBP iteration count equaled the number of 80.1-km spans. In this experiment, we tested 4 cases. First case is not applying nonlinearity compensation. Received data was demodulated without assistance by pilot-tone. Second and third cases used DBP and pilot-tone, respectively. The fourth used both techniques simultaneously. In the fourth case, pilot-tone aided phase noise compensation was performed after DBP. We evaluated subcarrier 4 (sc4) in ch3, and fiber launched power was varied from -7.5 dBm/ch to -1.5 dBm/ch. It was defined as the total power of a 538 Gb/s SC-FDM signal with

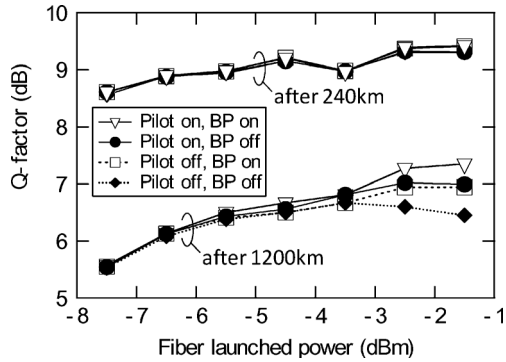

Fig. 13. Nonlinear tolerance in 7 ch WDM transmission with and without pilot-tone aided phase noise compensation and DBP (ch3, sc4).

8 subcarriers. Q-factor was calculated from BER of sc4 in ch3 (1549.32 nm). The nonlinear impairments on SC-FDM subcarriers are SPM, XPM between subcarriers in the same WDM channel and XPM between neighboring WDM channels. They also include the nonlinear interaction between the two polarization components. DBP is employed to compensate intra-channel nonlinear effects, and pilot-tone is utilized to compensate inter-channel nonlinear effects. Fig. 13 shows nonlinear tolerance in each case after 240 km and 1200 km transmission. At the shorter transmission distance of 240 km, all four cases exhibit comparable performance at each fiber launched power. At the launched power of -1.5 dBm, Q-factors are not improved by using nonlinearity compensation; they are limited by the OSNRs. On the other hand, at high launched powers of over -3.5 dBm/ch for 1200 km transmission, nonlinearity compensation techniques proved beneficial. At -1.5 dBm/ch, the Q-improvements with pilot-tone and DBP were 0.5 dB, because SPM was partly compensated when using DBP and inter-channel XPM was partially compensated when using pilot-tone. Since both nonlinear effects are compensated, Q-factor was improved by 1 dB when applying both techniques. Note that more improvement can be achieved by increasing DBP iteration, but computational complexity would drastically increase and benefit and complexity do not balance as shown in Fig. 1. In pilot-tone aided phase compensation technique, to accurately compensate phase noise due to inter-channel XPM, it is necessary to widen the guard band between the Nyquist-shaped signal and pilot-tone at the cost of a spectral efficiency [27].

D. Results of 7 × 538 Gb/s Long-Haul WDM Transmission

The transmission performance in the seven channel WDM configuration and single channel configuration were compared at the launched power of -2.5 dBm/ch. In these measurements, we utilized only pilot-tone aided phase noise compensation to improve nonlinear tolerance and DBP was not used. Q-factor dependence on transmission distance is shown in Fig. 14. Each plot shows the averaged Q-factor of the 8 subcarriers in the 538 Gb/s PDM-64QAM SC-FDM signal. The difference in Q-factors at shorter distances is mainly due to the linear cross talk triggered by the existence of neighboring WDM channels. As transmission distance increased, the Q-factor was decreased by inter-channel XPM, but the Q-factor degradation was

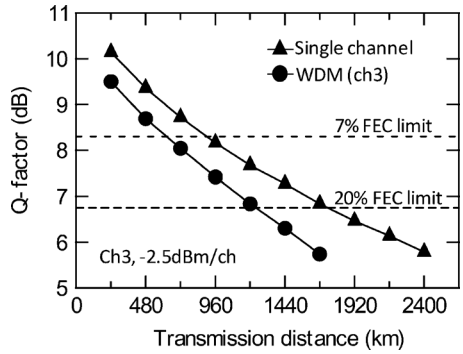

Fig. 14. Transmission performance with digital pilot-tone in single channel and WDM configuration.

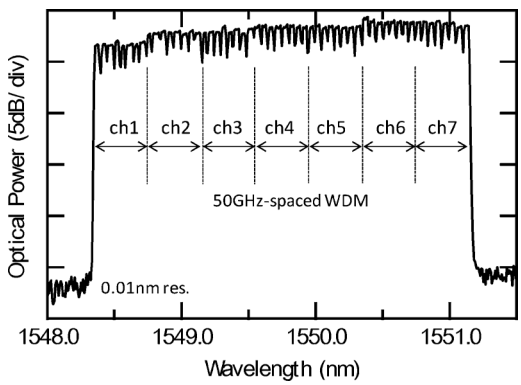

Fig. 15. Optical spectra of 50 GHz-spaced 7 ch WDM signal after 1200 km transmission.

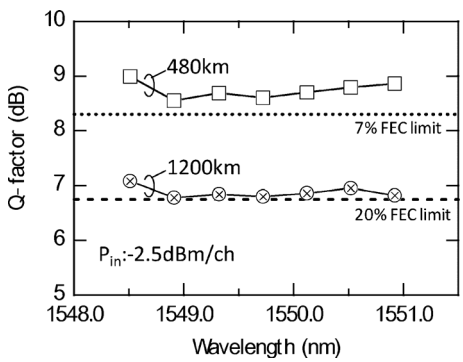

Fig. 16. Average Q-factors of 8 subcarriers of WDM channels after 480 km and 1200 km.

gradual, thanks to pilot-tone-aided phase noise compensation. In the single channel configuration, we achieved the distances of 720 km and 1680 km for the FEC limits of 7% and 20%, respectively.

The Q-factors of all 7 channels at the distances of 480 km and 1200 km were measured at average power of -2.5 dBm/ch. Fig. 15 shows the optical spectra of seven WDM channels with the spacing of 50 GHz after 1200 km transmission (0.01 nm resolution). The Q-factors calculated from the average BER of the 8 subcarriers in each WDM channel are shown in Fig. 16. Assuming the 7% FEC limit of 8.3 dB, we achieved 480 km transmission with the channel bit-rate of 503 Gb/s/ch and the spectral

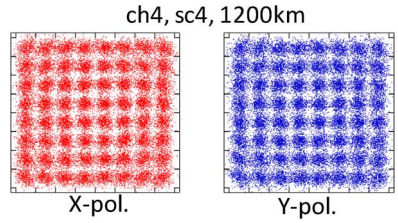

Fig. 17. Recovered constellations (32767 symbols) of sc4 in ch3 after 1200 km transmission.

efficiency of 10 b/s/Hz. Employing 20% overhead FEC, which has a Q-limit of 6.75 dB [16], 1200 km transmission is possible at the channel bit-rate of 448 Gb/s/ch with SE of 8.96 b/s/Hz. The recovered constellations of sc4 in ch3 for X- and Y-polarization after 1200 km transmission are shown in Fig. 17.

IV. C- and Extended L-Band 102.3 Tb/s WDM Transmission Experiments

Here, we conduct an ultra wide band WDM transmission experiment in the 11.2 THz of C- and L^+-band to confirm the feasibility of 100 Tb/s-class transport systems, which can accommodate high speed client signals of 400 G Ethernet with standard terrestrial repeater spacing of 80 km and WDM spacing of 50 GHz.

A. Experimental Setup

Fig. 18 shows the experimental setup. This is a modification of the 7 ch long-haul WDM setup. 224 CW optical carriers (1526.44–1565.09, and 1567.95–1620.94 nm) with 50-GHz spacing in the C- and extended L^+-bands were generated in the transmitter. ECL with a linewidth of about 60 kHz was employed under the measurement; the remaining lasers were DFB lasers. The odd/even channels were separately multiplexed, and each carrier was fed to a SC-FDM signal generator (structure is as shown in Fig. 6). In this experiment, we employed an electrical 5.71-Gbaud Nyquist-pulse-shaped 64QAM signal with a roll-off factor of 0.01 to achieve higher spectral efficiency and 100 Tb/s-class total capacity. The subcarrier number and spacing in each SC-FDM signal were 8 and 6.25 GHz, respectively, as in the long-haul transmission experiment. The even and odd SC-FDM signals then were combined by an optical coupler, and polarization multiplexed with 25-nsec delay. Consequently each 50-GHz spaced channel consisted of eight PDM-64QAM signals (6.25-GHz spacing) with line rate of 548 Gb/s, resulting in the SE of 9.1 b/s/Hz assuming 20% FEC overhead. Note that the pilot-tone attached to each subcarrier and was placed at 2.94 GHz from the center frequency of the subcarrier. Its optical spectrum, which was measured by an optical spectrum analyzer with the high frequency resolution of 55 MHz, is shown in Fig. 19. At the transmitter, we employed C- and L^+-band EDFAs [37] with parallel configuration to compensate the loss of the modulation sections; their gain characteristics were carefully tuned to obtain low-noise flat WDM signals. For the measured channel, we used a tunable ECL with a linewidth of about 60 kHz; the remaining lasers were DFB lasers (linewidth $\sim$2 MHz).

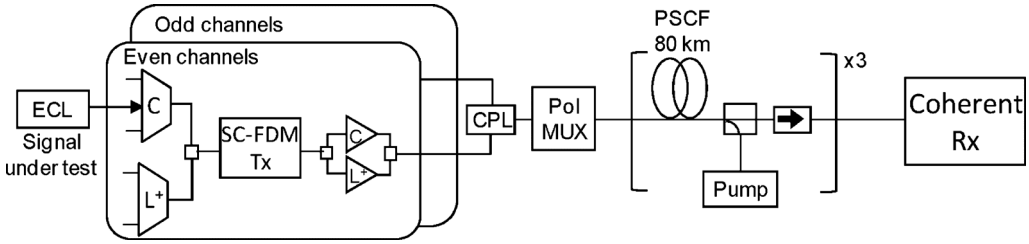

Fig. 18. Experimental setup for C- and L^+ WDM transmission.

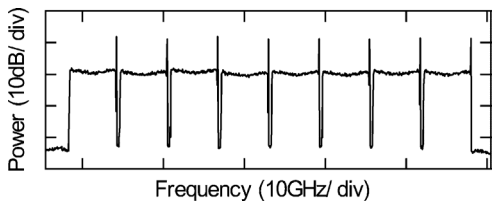

Fig. 19. Optical spectrum of a 548-Gb/8-subcarrier SC-FDM signal (6.25 GHz spacing).

The transmission line was a straight line consisting of the three 80.1-km spans of PSCF used in the 7 ch WDM transmission experiment. We utilized all-Raman amplification to compensate the losses of the transmission line; the backward-pumped DRA with 6 wavelengths, which were selected from 9 wavelengths (1422, 1430, 1440, 1450, 1460, 1470, 1480, 1490 and 1505 nm) at each span, yielded the on-off gain of 16 dB.

The receiver configuration shown in Fig. 4 was employed. The received signals were filtered by 0.5-nm and 0.1-nm OBPFs, and detected by a DPOH. We used a free-running ECL with a linewidth of ~70 kHz as the LO. Received signals were digitized at 80 GS/s using two synchronized digital storage oscilloscopes, and stored in sets of 4 M samples. Each subcarrier was individually post-processed offline using the same algorithm described in Section II. The tap number of the adaptive equalizer was 27. Pilot-tone-aided phase noise compensation was used in all measurements, and DBP was not applied. BER was calculated from the 1.5 Mbit demodulated signals.

B. Back-to-Back Measurements

We measured the tolerance to subcarrier spacing in the back-to-back configuration. This is tested in the 4-subcarrier 64-QAM SC-FDM configuration. The baud rate and the ONSR were set to 5.71 Gbaud and 28 dB, respectively. The wavelength of the test channel was 1545.32 nm. Fig. 20 shows the measurement results. The Q-factor was almost independent of the subcarrier spacing when the spacing was larger than 5.9 GHz ($1.042 \times$ Nyquist frequency), and the inter-subcarrier linear crosstalk can be ignored in this spacing range. The slight degradation in Q-factors at larger subcarrier spacing is attributed to the small increase in spurious components created during multi-carrier generation by MZM, see Fig. 6. On the other hand, Q-factors rapidly decreased when the spacing was below 5.9 GHz. In our WDM transmission experiment, the subcarrier spacing was fixed at 6.25 GHz (1/8 of the channel spacing),

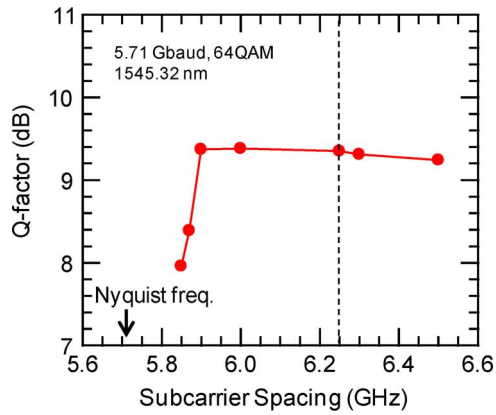

Fig. 20. Q-factor as a function of subcarrier spacing.

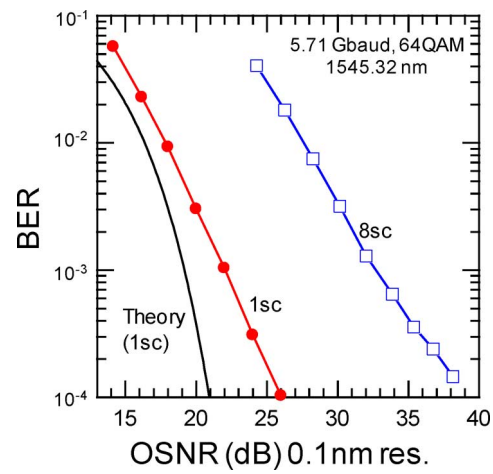

Fig. 21. OSNR tolerance of 1 sc, 8 sc in back-to-back configuration.

shown by the dashed line in Fig. 20, which confirms successful suppression of the inter-channel linear crosstalk caused by the frequency fluctuation of neighboring laser sources. Fig. 21 shows the measured back-to-back BER characteristics of single carrier and 8-subcarrier SC-FDM signals at the wavelength of 1545.32 nm. The required OSNR ($\mathrm{BER} = 1 \times 10^{-2}$) of a 1 sc Nyquist-filtered 64-QAM was17.9 dB, which is 1.6 dB off the theoretical limit of 64-QAM assuming AWGN. The required OSNR for an 8-subcarrier 548-Gb/s SC-FDM signal was 27.6 dB. The excess OSNR penalty due to subcarrier multiplexing was 0.7 dB, which was successfully suppressed thanks to tight Nyquist filtering with small roll-off factor of 0.01.

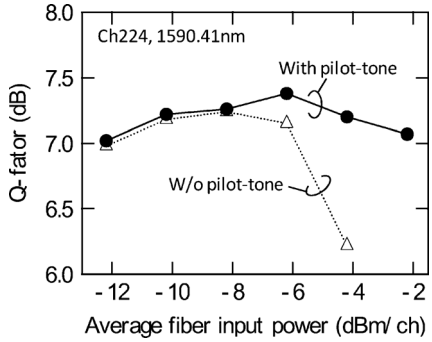

Fig. 22. Q-factor as a function of average input power after 240 km.

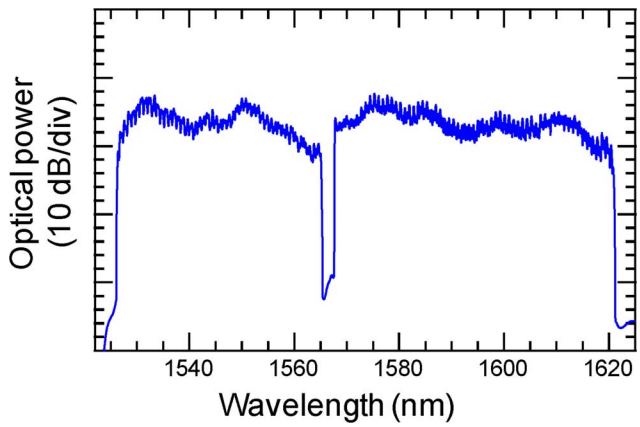

Fig. 23. Optical spectra after 240 km transmission.

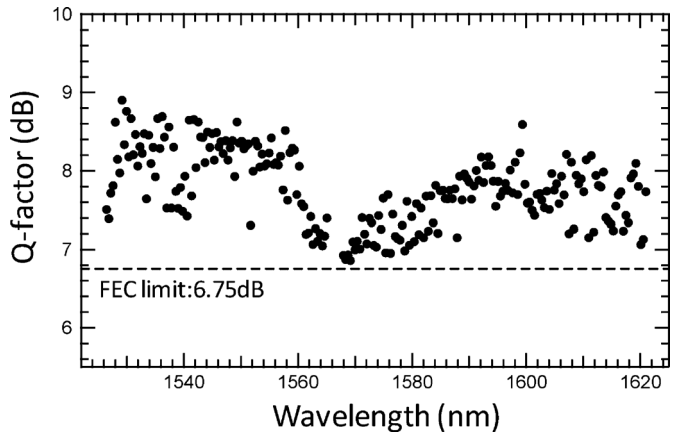

Fig. 24. Average Q-factors of 8 subcarriers of 224 WDM channels after 240 km at average input power of -8.2 dBm/ch.

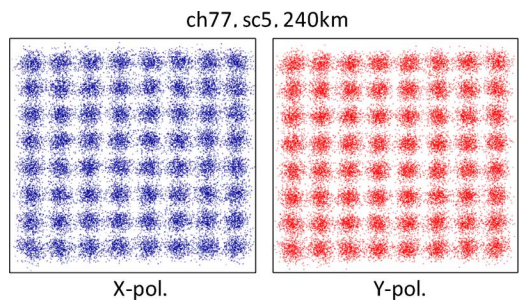

Fig. 25. Recovered constellations (32767 symbols) of both polarization tributaries of sc5 in ch77 after 240 km.

C. Transmission Results

To investigate optimal fiber launched power, we measured the fiber launched power tolerance with and without pilot-tone-aided phase noise compensation in 224 ch WDM 240 km transmission. The wavelength of the test channel was 1590.41 nm. The average power of the 224 WDM channels was varied from -12.2 dBm/ch to -2.2 dBm/ch in increments of 1 dB. Fig. 22 shows the fiber launched power dependence of the Q-factor after 240 km. With pilot tone, Q-factor increased in proportion to the launched power in the range of -12.2 dBm/ch to -6.2 dBm/ch. We confirmed stable convergence of demodulation processing in all measurements thanks to the phase noise compensation provided by the pilot-tone in ultra-wideband transmission. On the other hand, the measured Q-factors without pilot tone decreased rapidly due to nonlinear impairments when the average fiber input power exceeded -6.2 dBm/ch. In all channel measurements, taking account of the channel power deviation, the average power was set to -8.2 dBm/ch.

Finally, we measured the performance of 224-channel WDM transmission at the average fiber launched power of -8.2 dBm/ch. Fig. 23 shows the optical spectra after 240-km transmission measured with 0.2-nm resolution. The received OSNR values were around 29 dB thanks to the ultra-wideband all-Raman amplification over C-band (4.9 THz) and extended L-band (6.3 THz). The measured BER performance after 240-km transmission is shown in Fig. 24 and the recovered constellations of both polarization tributaries of sc5 in ch77 after 240 km are shown in Fig. 25. Each plot in Fig. 24 represents the Q-factor calculated from the average BER of the 8 subcarriers. Q-factors of all 224 channels were confirmed to be better than 6.86 dB, which exceeds the Q-limit of 6.75 dB (dashed line) with the use of today's continuously interleaved BCH hard decision FEC techniques (20% overhead) [16].

V. Conclusion

In this paper, we described nonlinear tolerant PDM 64-QAM SC-FDM with pilot-tone use for high- spectrally-efficient and high capacity transmission systems accommodating future 400 G Ethernet transport.

We investigated the long-haul transmission performance of 7×538 Gb/s PDM-64QAM SC-FDM signals. 480 km transmission at SE of 10 b/s/Hz and 1200 km transmission at SE of 8.96 b/s/Hz were achieved assuming 7% and 20% FEC overhead, respectively, thanks to the high-speed channel generation realized by SC-FDM with tight Nyquist-pulse-shaping and nonlinear tolerance enhancement by pilot-tone-aided phase noise compensation. It can effectively improve the transmission characteristics of 400 Gb/s-class SC-FDM signals with less computational complexity than demanded by nonlinearity compensation based on DBP.

We also demonstrated the 102.3 Tb/s WDM transmission using 50-GHz spaced 548-Gb/s PDM 64-QAM SC-FDM signals enhanced by pilot-tone aided phase noise compensation. The transmission distance of over 3×80 km, the longest reported for 100-Tb/s-class transmission, was attained with

the spectral efficiency of 9.1 b/s/Hz, and the ultra-wide band all-Raman amplification in the C- and extended L-bands realized the total signal bandwidth of 11.2 THz.

These results show the feasibility of 100 Tb/s-class WDM transmission with 400-Gb/s channels while maintaining the compatibility with conventional WDM spacing of 50 GHz and terrestrial repeater spacing of 80 km.

ACKNOWLEDGMENT

The authors would like to thank K. Hagimoto, A. Takahara, S. Suzuki, K. Okada for their constant encouragement and fruitful discussions. Thanks are due to H. Masuda, S. Yamanaka, H. Kawakami, M. Mizoguchi, T. Nakagawa, R. Kou, M. Yoshida, S. Okamoto, S. Yamamoto, T. Sakano, N. Fujiwara, K. Horikoshi for fruitful discussions and technical support.

REFERENCES

[1] Y. Miyamoto, A. Sano, and T. Kobayashi, "The challenge for the next generation OTN based on 400 Gbps and beyond," in *Proc. OFC/NFOEC*, 2012, paper NTu2e.3.

[2] T. Kobayashi, A. Sano, M. Yoshida, T. Sakano, H. Kubota, Y. Miyamoto, K. Ishihara, M. Mizoguchi, and M. Nagatani, "45.2 Tb/s C-band WDM transmission over 240 km using 538 Gb/s PDM-64QAM single carrier FDM signal with digital pilot tone," in *Proc. ECOC*, 2011, paper Th13.C.6.

[3] H. Takahashi, K. Takeshima, I. Morita, and H. Tanaka, "400-Gbit/s optical OFDM transmission over 80 km in 50-GHz frequency grid," in *Proc. ECOC*, 2010, paper Tu.3.C.1.

[4] X. Zhou, L. Nelson, P. Magill, R. Isaac, B. Zhu, D. W. Peckham, P. Borel, and K. Carlson, "4000 km transmission of 50 GHz spaced, 10 494.85-Gb/s hybrid 32–64QAM using cascaded equalization and training-assisted phase recovery," in *Proc. OFC*, 2012, paper PDP5C.6.

[5] S. Chandrasekhar, X. Liu, B. Zhu, and D. W. Peckham, "Transmission of a 1.2-Tb/s 24-carrier no-guard-interval coherent OFDM superchannel over 7200-km of ultra-large-area fiber," in *Proc. ECOC*, 2009, paper PD2.6.7.

[6] W. Shieh and I. Djordjevic*, OFDM for Optical Communications*. New York: Academic, 2009.

[7] S. L. Jansen, I. Morita, T. C. W. Schenk, N. Takeda, and H. Tanaka, "Coherent optical 25.8-Gb/s OFDM transmission over 4160-km SSMF," *J. Lightw. Technol.*, vol. 26, no. 1, pp. 6–15, Jan. 2008.

[8] X. Liu, S. Chandrasekhar, B. Zhu, P. J. Winzer1, A. H. Gnauck, and D. W. Peckham, "Transmission of a 448-Gb/s reduced-guard-interval CO-OFDM signal with a 60-GHz optical bandwidth over 2000 km of ULAF and five 80-GHz-grid ROADMs," in *Proc. OFC*, 2010, paper PDPC2.

[9] K. Ishihara, T. Kobayashi, R. Kudo, Y. Takatori, A. Sano, and Y. Miyamoto, "Frequency-domain equalization for coherent optical single-carrier transmission systems," *IEICE Trans. Commun.*, vol. E92 B, no. 12, pp. 3736–3743, 2009.

[10] T. Kobayashi, A. Sano, E. Yamada, E. Yoshida, and Y. Miyamoto, "Over 100 Gb/s electro-optically multiplexed OFDM for high-capacity optical transport network," *J. Lightw. Technol.*, vol. 27, no. 16, pp. 3714–3720, Aug. 2009.

[11] W. Shieh and Y. Tang, "Ultrahigh-speed signal transmission over nonlinear and dispersive fiber optic channel: The multicarrier advantage," *IEEE Photon. J.*, vol. 2, no. 3, pp. 276–283, 2010.

[12] S. L. Jansen, "Multi-carrier approaches for next-generation transmission: Why, where and how?," in *Proc. OFC*, 2012, paper OTh1B.

[13] H. G. Myung, J. Lim, and D. J. Goodman, "Single carrier FDMA for uplink wireless transmission," *IEEE Vehic. Tech. Mag.*, vol. 1, pp. 30–38, 2006.

[14] Y. Tang, W. Shieh, and B. S. Krongold, "DFT-spread OFDM for fiber nonlinearity mitigation," *IEEE Photon. Technol. Lett.*, vol. 22, no. 16, pp. 1250–1252, 2010.

[15] A. Li, X. Chen, G. Gao, A. Al Amin, W. Shieh, and B. S. Krongold, "Transmission of 1.63-Tb/s PDM-16QAM unique-word DFT-spread-OFDM signal over 1 010-km SSMF," in *Proc. OFC*, 2012, paper OW4C.1.

[16] 100 G CI-BCH-4TM eFEC Technology [Online]. Available: www.vitesse.com

[17] Y. Miyata, K. Sugihara, W. Matsumoto, K. Onohara, K. Kubo, H. Yoshida, and T. Mizuochi, "A triple-concatenated FEC using soft-decision decoding for 100 Gb/s optical transmission," in *Proc. OFC/NFOEC*, 2010, paper OThL3.

[18] K. Kikuchi, M. Fukase, and S.-Y. Kim, "Electronic post-compensation for nonlinear phase in a 1000-km 20-Gbit/s optical QPSK transmission system using the homodyne receiver with digital signal processing," in *Proc. OFC/NFOEC*, 2007, paper OTuA2.

[19] E. Ip and J. M. Kahn, "Compensation of dispersion and nonlinear impairments using digital backpropagation," *J. Lightw. Technol.*, vol. 26, no. 20, pp. 3416–3425, Oct. 2008.

[20] L. Li, Z. Tao, L. Dou, W. Yan, S. Oda, T. Tanimura, T. Hoshida, and J. C. Rasmussen, "Implementation efficient nonlinear equalizer based on correlated digital backpropagation," in *Proc. OFC*, 2011, paper OWW3.

[21] E. Yamazaki, H. Masuda, A. Sano, T. Yoshimatsu, T. Kobayashi, E. Yoshida, Y. Miyamoto, R. Kudo, K. Ishihara, M. Mtsui, and Y. Takatori, "Multi-staged nonlinear compensation in coherent receiver for 12 015 km WDM transmission of 10-ch × 111 Gbit/s noguard-interval co-OFDM," *Electron. Lett.*, vol. 45, no. 31, pp. 695–697, 2009.

[22] E. Yamazaki, A. Sano, T. Kobayashi, W. Yoshida, and Y. Miyamoto, "Mitigation of nonlinearities in optical transmission systems," in *Proc. OFC*, 2011, paper OThF1.

[23] R. Weidenfeld, M. Nazarathy, R. Noe, and I. Shpantzer, "Volterra nonlinear compensation of 112 Gb/s ultra-long-haul coherent optical OFDM based on frequency-shaped decision feedback," in *Proc. ECOC*, 2009, paper 2.3.3.

[24] F. P. Guiomar, J. D. Reis, A. Teixeira, and A. N. Pinto, "Mitigation of intra-channel nonlinearities using a frequency-domain volterra series equalizer," in *Proc. ECOC*, 2011, paper Tu.6.B.1.

[25] E. Ip, Y.-K. Huang, E. Mateo, Y. Aono, Y. Yano, T. Tajima, and T. Wang, "Inter channel nonlinearity compensation for $3\lambda \times 114$-Gb/s DP-8QAM using three synchronized sampling scopes," in *Proc. OFC*, 2012, paper OM3A.6.

[26] B. Inan, S. Randel, S. L. Jansen, A. Lobato, S. Adhikari, and N. Hanik, "Pilot-tone-based nonlinearity compensation for optical OFDM systems," in *Proc. ECOC*, 2010, paper Tu.4.A.6.

[27] L. Du and A. Lowery, "Experimental demonstration of pilot-based XPM nonlinearity compensator for CO-OFDM systems," in *Proc. ECOC*, 2011, paper Th.11.B.4.

[28] A. Diaz, A. Napoli, S. Adhikari, Z. Maalej, A. Lobato, M. Kuschnerov, and J. Prat, "Analysis of back-propagation and RF pilot-tone based nonlinearity compensation for a 9×224 Gb/s POLMUX-16QAM system," in *Proc. OFC*, 2012, paper OTh3C.5.

[29] R. Kudo, T. Kobayashi, K. Ishihara, Y. Takatori, A. Sano, and Y. Miyamoto, "Coherent optical single carrier transmission using overlap frequency domain equalization for long-haul optical systems," *J. Lightw. Technol.*, vol. 27, no. 16, pp. 3721–3728, Aug. 2009.

[30] T. Kobayashi, A. Sano, A. Matsuura, E. Yamazaki, E. Yoshida, Y. Miyamoto, T. Nakagawa, Y. Sakamaki, and T. Mizuno, "120-Gb/s PDM 64-QAM transmission over 1 280 km using multi-staged nonlinear compensation in digital coherent receiver," in *Proc. OFC*, 2011, paper OThF6.

[31] T. Kobayashi, A. Sano, A. Matsuura, Y. Miyamoto, and K. Ishihara, "Nonlinear tolerant long-haul WDM transmission over 1200 km using 538 Gb/s/ch PDM-64QAM SC-FDM signals with pilot tone," in *Proc. OFC2012*, 2012, paper OM2A.

[32] A. Sano, T. Kobayashi, S. Yamanaka, A. Matsuura, H. Kawakami, Y. Miyamoto, K. Ishihara, and H. Masuda, "102.3-Tb/s (224×548-Gb/s) C- and extended L-band all-Raman transmission over 240 km using PDM-64QAM single carrier FDM with digital pilot tone," in *Proc. OFC*, 2012, paper PDP5C.

[33] K.-C. Hung and D. W. Lin, "Joint carrier recovery and multimodulus blind decision-feedback equalization under high-order QAM," in *Proc. GLOBECOM*, 2004, pp. 2281–2285.

[34] J. Yang, J.-J. Werner, and G. A. Dumont, "The multimodulous blind equalization and its generalized algorithms," *IEEE J. Sel. Areas Commun.*, vol. 20, no. 5, pp. 997–1015, May 2002.

[35] S. J. Savory, "Digital filters for coherent optical receivers," *Opt. Exp.*, vol. 16, no. 2, pp. 804–817, 2008.

[36] K. Yonenaga, A. Sano, E. Yamazaki, F. Inuzuka, Y. Miyamoto, A. Takada, and T. Yamada, "100 Gbit/s all-optical OFDM transmission using 4×25 Gbit/s optical duobinary signals with phase-controlled optical sub-carriers," in *Proc. OFC*, 2008, paper JThA48.

[37] H. Masuda and Y. Miyamoto, "Low-noise extended L-band phosphorus co-doped silicate EDFA consisting of novel two-stage gain-flattened gain blocks," *Electron. Lett.*, vol. 44, no. 18, p. 1082, 2008.

Takayuki Kobayashi (M'08) received the B.E. and M.E. degrees in communications engineering from Waseda University, Tokyo, Japan, in 2004 and 2006, respectively.

Since April 2006, he has been with NTT Network Innovation Laboratories, NTT, Yokosuka, Japan. His current research interests are spectrally-efficient modulation formats enhanced by digital signal processing and large-capacity fiber-optic communications systems.

Akihide Sano (M'08) received the B.S. and M.S. degrees in physics and Ph.D. degree in communication engineering from Kyoto University, Kyoto, Japan, in 1990, 1992, and 2007, respectively.

In 1992, he joined the NTT Transmission Systems Laboratories, Yokosuka, Kanagawa, Japan, where he was engaged in research and development on high-speed optical communication systems. His current research interests include large-capacity long-haul fiber-optic communication systems.

Dr. Sano received the Best Paper Award of the First Optoelectronics and Communication Conference (OECC'96) in 1996, the Young Engineer Award in 1999, and the Achievement Award in 2010 from IEICE.

Akihiko Matsuura received his B.E. degree from the Tokyo University of Science in 1995, and the M.E. degree from Tokyo Institute of Technology in 1997. Since 1997 he has been with NTT Laboratories, where he researched 40 G optical transmission, submarine transmission systems, and digital coherent transmission.

Yutaka Miyamoto (M'93) received the B.E. degree and M.E. degree in electrical engineering from Waseda University, Tokyo, Japan, in 1986 and 1988, respectively.

In 1988, he joined the NTT Transmission Systems Laboratories, Yokosuka, Japan, where he engaged in research and development on 10 Gbit/s terrestrial optical communications systems with EDFA. He is now a Senior Distinguished Researcher and the group leader of NTT Network Innovation Laboratories. His current research interest includes high-capacity optical transport network with advanced modulation formats and digital signal processing.

Dr. Miyamoto is a Fellow of the Institute of Electronics, Information and Communication Engineers (IEICE) of Japan. He received the best paper award from the IEICE Communication Society in 2003, the 23rd Kenjiro Sakurai Memorial Prize from OITDA in 2007, and the Achievement Award from IEICE in 2010.

Koichi Ishihara (M'06) received the B.E., M.E,. and Ph.D. degrees in communications engineering from Tohoku University, Sendai, Japan, in 2004, 2006 and 2011, respectively.

Since April 2006, he has been with NTT Network Innovation Laboratories, Yokosuka, Japan. His current research interests include digital signal transmission techniques for broadband wireless and fiber-optic communication systems.

Dr. Ishihara is a member of the Institute of Electronics, Information and Communication Engineers (IEICE) of Japan. He received the Young Engineer Award from the IEICE in 2009, and the 2011 IEICE RCS (Radio Communication Systems) Active Research Award in 2011.